Journal of Sustainable Metallurgy
https://doi.org/10.1007/s40831-023-00778-y

RESEARCH ARTICLE

Insights into the Valorization of Electric Arc Furnace Slags as Supplementary Cementitious Materials

Anton Andersson[1] · Jenny Isaksson[1] · Andreas Lennartsson[1] · Fredrik Engström[1]

Received: 16 October 2023 / Accepted: 6 December 2023

Abstract

The transition to hydrogen-based reduction processes within the iron and steelmaking industry will generate new types of slag compositions that require valorization routes. Using slags as supplementary cementitious materials (SCMs) addresses the carbon dioxide emissions of the cement industry since the SCM requires neither calcination nor clinkering. Conventionally, ironmaking slags from the blast furnace (BF) are recycled as SCMs, i.e., ground granulated BF slag (GGBS). Ideally, future slags from electric arc furnaces (EAFs) operating on hydrogen-based direct reduced iron should be valorized analogously. Since the hydrogen-based process route is not yet realized in an industrial scale, the literature lacks data to support this valorization route, and additionally, literature on scrap-based EAF slags is scarce. Therefore, the present study aimed to offer insights into the utilization of ore-based EAF slags as SCMs based on an industrial slag sample from an EAF operating on hot briquetted iron. The slag was remelted, modified, and water-granulated in laboratory scale, and its performance as an SCM was compared to water-granulated ladle slag and two commercial GGBS. The results showed promising reactivities measured using the R^3 isothermal calorimeter-based testing protocol. Based on the comparison to GGBS, the study indicated that generating reactive and appropriate SCMs from EAF slags will partly be a challenge in balancing the crystallization of the MeO-type solid solution rich in magnesia and addressing the iron oxide content in the amorphous phase.

The contributing editor for this article was Sharif Jahanshahi.

✉ Andreas Lennartsson
andreas.lennartsson@ltu.se

Anton Andersson
anton.andersson@ltu.se

Jenny Isaksson
jenny.isaksson@ltu.se

Fredrik Engström
fredrik.i.engstrom@ltu.se

[1] Division of Minerals and Metallurgical Engineering, Luleå University of Technology, 971 87 Luleå, Sweden

Published online: 26 December 2023

Graphical Abstract

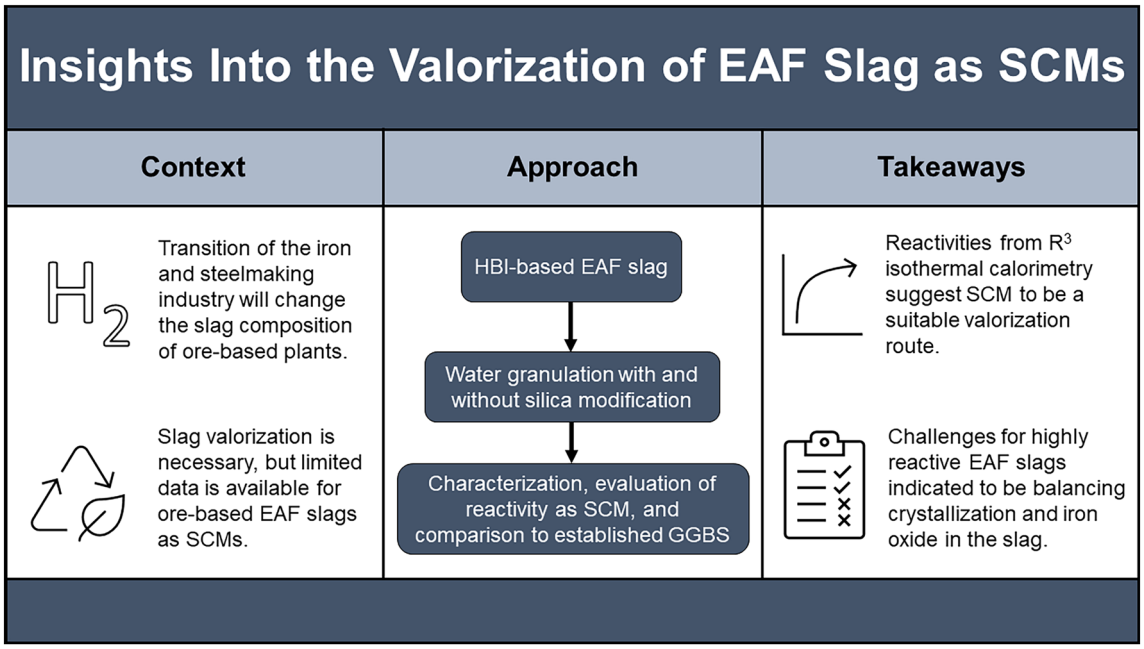

Keywords Electric arc furnace slag · Supplementary cementitious material · Slag valorization · Sustainability · Circularity

Introduction

The iron and steelmaking industry accounts for approximately 7% of the anthropogenic carbon dioxide emissions [1]. In recent years, initiatives to move away from the carbon-intensive blast furnace (BF) route have emerged; one such initiative is HYBRIT [1]. An implication of this transition to hydrogen-based reduction processes is a change in future slag streams in ore-based steelmaking plants. In Europe, BF slag is recycled to the extent of 100%, out of which 80% is in cement and concrete applications [2]. For steel producers aiming to use an electric arc furnace (EAF) to smelt the direct reduced iron [1], a slag valorization route for the EAF slag must be considered to maintain sustainable steel production from a material efficiency standpoint.

Currently, EAF slags have multiple external application areas, including fertilizers, water purification, and different construction applications where road construction is dominating [2, 3]. Although external applications are in place, the ambition to shift the ore-based ironmaking process and the subsequent increase in the total volume of EAF slag justifies a reassessment of the slag valorization route.

Similar to the iron and steelmaking industry, the production of cement is a major contributor to anthropogenic carbon dioxide emissions. Roughly 6–8% of the total global emissions are attributed to the cement industry [4]. In Portland cement, 60% of the emissions stem from the release of carbon dioxide during the calcination of limestone, while 40% are related to fuels and electricity used in heating and milling [4]. By partially replacing cement with a supplementary cementitious material (SCM), the carbon dioxide emissions per ton of cementitious material are reduced since the SCM requires neither calcination nor clinkering [5]. In addition, the requirements for quarrying of limestone are reduced. Therefore, transitioning the EAF slag valorization route to an SCM is of interest.

Partially replacing cement with an SCM influences the amount and kind of hydrates formed upon cement hydration, which was reviewed by Lothenbach et al. [5]. In cement pore solution conditions, SCMs show either pozzolanic activity, hydraulic properties, or a combination of both [4]. Depending on the method used for evaluating the reactivity of SCMs, the reactivity value can be correlated to the compressive strength of mortars [6].

There are several documented factors affecting SCM reactivity. Crystalline phases, other than traditional cement clinker phases, are generally considered inert with few exceptions, such as zeolites [7–9]. Thus, an amorphous material is a prerequisite for most SCMs. The composition of the amorphous material affects reactivity by the presence of elements participating in the cementitious reactions and by affecting the degree of polymerization of the glass. Ramanathan et al. [10] used dissolution experiments to show that the elemental release of silicon and aluminum correlated to

the reactivity of the SCM. In addition, calcium can provide hydraulic properties of the SCM [4]. Furthermore, more depolymerized amorphous phases show higher reactivities [4, 11], which relates to the types and concentrations of network forming and breaking oxides in the silicate network. The thermal history of the SCM plays a role in the reactivity [4], which translates to, e.g., air or water granulation of a slag. Finally, the specific surface area is a key parameter as the dissolution in the cement pore solution is a surface reaction, and, in addition, more particles provide a higher number of nucleation sites for reaction products [4, 10, 12].

Since crystalline phases are generally considered inert, and assuming that the crystalline phases typical for slowly cooled EAF slags lack hydraulic properties, generating a reactive EAF slag necessitates water granulation to form an amorphous material. This is evident when reviewing available literature on slowly cooled EAF slags [13, 14]. The two slags included in the study by Rojas and Sánchez de Rojas [13] showed no pozzolanic activity. The same results were found by Hekal et al. [14], although they did not present the cooling procedure of the slag or the crystalline phases present. As EAF slag is traditionally cooled in slag heaps, the literature not presenting the phase distribution can be assumed to study predominantly crystalline slags.

Spraying water on the tapped EAF slag generated a material with a mixture of crystalline and amorphous phases [15]. The partial replacement of cement with this slag generated a slightly positive impact on mortar compressive strength [15]. The same performance can be attributed to the EAF slag tested by Alsheltat and Elfigih [16]. Furthermore, Lee et al. [17] showed that a 15% replacement ratio of an EAF slag did not negatively affect the compressive strength of mortars after 28 days of curing. The two latter studies did not include information on the slags' phase distributions and were assumed to be crystalline [16, 17].

Although a slight positive effect could be attributed to the EAF slag, the reported studies neglected the use of a filler reference sample [15–17]. Therefore, the actual effect might be attributed to the filler effect rather than a contribution from the slag as an SCM. This is evident based on the data presented by Amin et al. [18], where scanning electron microscopy with energy dispersive spectroscopy (SEM–EDS) was employed on hydrated samples, including EAF slag, to conclude that the mechanism of improvement in strength was as a filler. Nonetheless, Roslan et al. [19] provided data from calcium hydroxide consumption experiments concluding the presence of pozzolanic activity of an EAF slag. They suggested that the slag was partly crystalline and partly amorphous [19], which might explain the pozzolanic activity.

There are three studies available on granulated EAF slag [15, 20, 21]. However, all slags are in some way engineered, i.e., not representing the actual slag from the furnace. Nonetheless, these studies offer insights into the possibility of using modified EAF slags as SCMs.

Muhmood et al. [15] remelted an EAF slag in a graphite crucible and tapped the liquid slag into a stagnant water bath. The resulting slag phase was significantly reduced in iron content, but the quenching failed, generating a crystalline slag with no pozzolanic properties [15]. Kim et al. [20] reduced an EAF slag, removing the majority of the iron while dissolving alumina from the crucible used in their experimental setup. The subsequent water quenching generated an entirely amorphous slag with excellent prospects for utilization as an SCM [20]. Finally, Bullerjahn and Bolte [21] presented an engineered EAF slag, retained in iron content but with a higher than usual polymerization degree for EAF slags, with an amorphous content of 87.5%. Their results demonstrated that it is possible to generate an SCM based on an EAF slag [21].

Based on the above, multiple studies on EAF slags aimed at SCM applications are performed on crystalline slags, i.e., not fulfilling the basic requirement for generating a reactive material. Furthermore, the amorphous EAF slags are exclusively metallurgically engineered. In addition, the engineered slags are not compared to the performance of the original EAF slag. Therefore, the present study aims to present a first insight into the reactivity of a water-granulated EAF slag and its relation to the reactivity of the engineered counterpart. For this purpose, an industrial EAF slag from a steelmaking process mainly based on hot briquetted iron (HBI) was remelted and modified with silica in laboratory scale to assess the influence of B2 (wt% CaO/wt% SiO_2) basicity on the inherent reactivity measured using the R^3 isothermal calorimeter protocol. By using an HBI-based slag rather than a scrap-based slag, the study includes a more relevant composition in terms of the elemental distribution corresponding to future steelmaking slags.

Methods

Sample Preparation

A spot sample of solidified and screened (< 25 mm) EAF slag was collected from a steel producer operating the EAF on HBI. In addition, a spot sample of solidified and screened (< 25 mm) ladle slag was collected and included in the study as a comparative material. The slag handling in the industry accounted for the entrained metallic phase and the resulting oxidic slags were used to generate four samples included in the study: a non-modified EAF slag, two silica-modified EAF slags, and a non-modified ladle slag. Table 1 summarizes the labeling of the samples and the modification of the B2 basicity.

Table 1 List of samples generated in the study

Label	Modifying agent	B2 basicity
EAF 2.0	None	As received
EAF 1.5	SiO_2 (99.5%)	1.5
EAF 1.0	SiO_2 (99.5%)	1.0
Ladle slag	None	As received

Since the amorphous content was identified as a key parameter in SCM applications, the slowly cooled industrial slags were remelted and water granulated in laboratory-scale experiments. The four samples summarized in Table 1 were transferred to molybdenum (tzm molybdenum 364) crucibles and remelted under an inert atmosphere in a graphite resistance-heated furnace (Ruhstrat, Göttingen, Germany), Fig. 1. Sample sizes of 200 g were used, and the inert atmosphere was attained by injecting argon (99.999% Ar) and nitrogen (99.996% N_2) at flow rates of 3 L/min and 12 L/min ambient temperature and pressure, respectively. The slag or silica-mixed slag samples were heated to 1873 K at a heating rate of 10 K/min and homogenized at 1873 K for 60 min.

Following the homogenization, the crucible was removed manually from the furnace, and the slag was tapped into water jets operating with cold tap water with a flow rate of 1.1 L/s. The granulation equipment is illustrated in Fig. 2

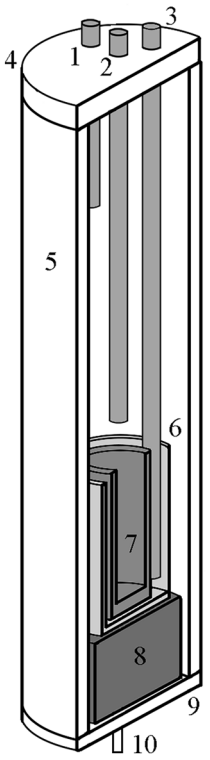

1. N_2 2 L/min
2. Ar 3 L/min
3. S-type thermocouple
4. Lid, not gas tight
5. Graphite working tube
6. Al_2O_3 crucible
   - Outer diameter 85 mm
   - Inner diameter 80 mm
   - Outer height 105 mm
   - Inner height 100 mm
7. Mo crucible
   - Outer diameter 60 mm
   - Inner diameter 50 mm
   - Outer height 100 mm
   - Inner height 90 mm
8. Graphite gas distributor
9. Bottom plate
10. N_2 10 L/min

Fig. 1 Experimental setup used for remelting the samples

1. Granulation box, 2. Tank cover, 3. Viewing window, 4. Water inlet, 5. Distributor for nozzles, 6. Tapping tube, 7. Water outlet to sieve

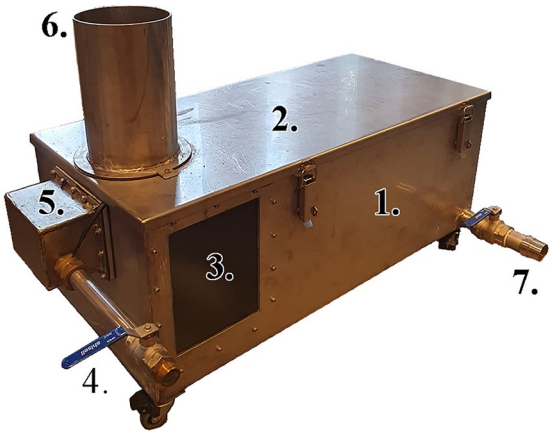

Fig. 2 Illustration of water granulation equipment

and an additional illustration of the granulation box is provided elsewhere [22]. The viewing window was utilized to ensure that all slag hit the water jets. In the experiments, the time between removing the crucible from the furnace and the first contact with the water jets was kept within 15 s.

Characterization

The original slag samples, i.e., prior to remelting and granulation, were subjected to X-ray fluorescence spectroscopy analyses (Thermo ARL 9900, Thermo Fisher Scientific, Waltham, MA, USA). Furthermore, the chemical compositions of the water-granulated samples were analyzed using the same equipment.

Rietveld powder X-ray diffraction (XRD) with an internal standard was used to estimate the amorphous content of the slags. Based on possible present phases, corundum (99.9%) was determined to be a suitable internal standard to avoid overlapping peaks. In accordance with the published literature [10, 23, 24], the chosen internal standard was mixed to obtain 10 wt% in the samples. Mixing was performed using a ring mill, and the subsequent scans were performed with a Malvern Panalytical Empyrean X-ray diffractometer (Malvern Panalytical, Malvern, UK) operating on copper K_α generated at 45 kV and 40 mA. The scans were performed between 10 and 90°2θ with a step size of 0.0130°2θ and a scan time per step of 698 s. The refinement was performed using HighScore + and the FIZ Karlsruhe inorganic crystal structure database.

The mineralogical characterization was complemented by studying the non-milled slag granules using SEM–EDS. Each sample of water-granulated slag was mounted in epoxy, polished using standard metallographic procedures, and carbon

coated. The analyses were performed with a Gemini Zeiss Merlin field emission SEM (Carl Zeiss AG, Oberkochen, Germany) equipped with a silicon drift EDS detector (Oxford Instruments, Abingdon, UK).

Reactivity Experiments

The samples were milled iteratively to a similar specific surface area using a FRITSCH Pulverisette 7 planetary ball mill (FRITSCH GmbH, Idar-Oberstein, Germany) equipped with 45 mL tungsten carbide grinding bowls. The samples were milled using 18 tungsten carbide balls of 10 mm in diameter at 600 RPM. The Brunauer, Emmet, and Teller (BET) specific surface area was measured using a Micromeritics Gemini 2390a after degassing at 573 K for 60 min using a Micromeritics FlowPrep 060 (Micromeritics Instruments Corporation, Norcross, GA, USA).

The milled samples were subjected to the isothermal calorimetry-based rapid screening test for SCMs outlined by Snellings and Scrivener [25], further developed and referred to as the rapid, relevant, and reliable (R^3) test by Avet et al. [26]. This method was chosen based on the study presented by Li et al. [6], which demonstrated that the R^3 test results correlated strongly with the strength of mortars, independent of the type of SCM and with great repeatability between laboratories. Furthermore, this calorimetry-based testing method tests the inherent reactivity of the SCM without the influence of cement hydration [27, 28].

Each individual sample was mixed on a dry basis with portlandite (98% $Ca(OH)_2$) and calcite (99.5% $CaCO_3$) according to the ratios presented by Li et al. [6]. Subsequently, the solid blends were mixed with a solution of potassium hydroxide containing potassium sulfate prepared according to Li et al. [6]. Pastes with 1.2:1 mass-based ratios of the liquid:solid blends were mixed for 2 min at 1600 RPM using an overhead stirrer. About 15 g of the paste was transferred to calorimeter glass ampoules and subsequently placed in a TAM Air isothermal calorimeter (TA Instruments, New Castle, DE, USA). The sealed ampoules were placed in the calorimeter within 5 min after adding the potassium hydroxide solution to the solid blend. The heat flow was recorded for 7 days at a temperature of 313.15 K.

The same R^3 protocol was employed for two commercial ground granulated blast furnace slag (GGBS) samples, labeled GGBS1 and GGBS2, and an inert reference of quartz. The chemical compositions of the GGBS, reported by the manufacturers, are shown in Table 2.

Table 2 Chemical composition [wt%] of the two GGBS samples

Sample	GGBS1	GGBS2
CaO	42.9	36.3
SiO_2	37.0	37.0
MgO	8.2	10.9
Al_2O_3	10.5	13.8
FeO	0.7	0.3
S	0.7	1.7

Results and Discussion

Chemical Composition After Water Granulation

The chemical compositions of the EAF and ladle slags prior to remelting and granulation are included in Fig. 3 and labeled original. In addition to the constituents included in Fig. 3, the original EAF slag contained 3.8, 1.1, 0.8, and 0.1 wt% MnO, TiO_2, Cr_2O_3, and V_2O_5, respectively.

Remelting and granulating the EAF slag without silica modification had less effect on the stable oxides of CaO, SiO_2, MgO, and Al_2O_3 (Fig. 3); the calculated B2 basicity shifted from 2.0 to 2.1, which could constitute the error margin of the analysis. However, the FeO content was significantly reduced upon remelting in the molybdenum crucible. Since the approach of using molybdenum crucibles is less common, the latter phenomenon was addressed.

Considering the binary Fe-Mo phase diagram in Fig. 4, iron is readily soluble in molybdenum at 1873 K. The information in the diagram suggests that close to 15 wt% of iron can dissolve into the molybdenum solid solution (ss) before forming intermediates. Forming intermediates would generate a diffusion barrier in the crucible and lower the interaction rate with the slag phase.

A simplified reaction can be proposed for the interaction between the ferrous oxide in the slag phase and the molybdenum crucible, and this reaction is presented in Eq. 1. The molybdenum crucible reduces the ferrous oxide, and iron forms the solid solution with molybdenum. To maintain the oxygen balance, every third of reduced ferrous iron must translate to MoO_3 entering the slag.

$$(FeO)_{Sl} + Mo(s) \leftrightarrow Mo(ss) + \left(MoO_3\right)_{Sl} \quad (1)$$

Considering the oxygen potential diagram in Fig. 5, the oxides CaO, Al_2O_3, MgO, and SiO_2 are significantly more stable than MoO_3, whereafter they are unaffected by the crucible. However, although FeO is more stable than MoO_3, these two oxides are closer to each other in the diagram. Furthermore, isolating the experimental temperature and including other oxidation states of iron and molybdenum revealed that, at 1873 K, the oxides are most stable in descending order according to FeO, Fe_3O_4, MoO_2, Fe_2O_3,

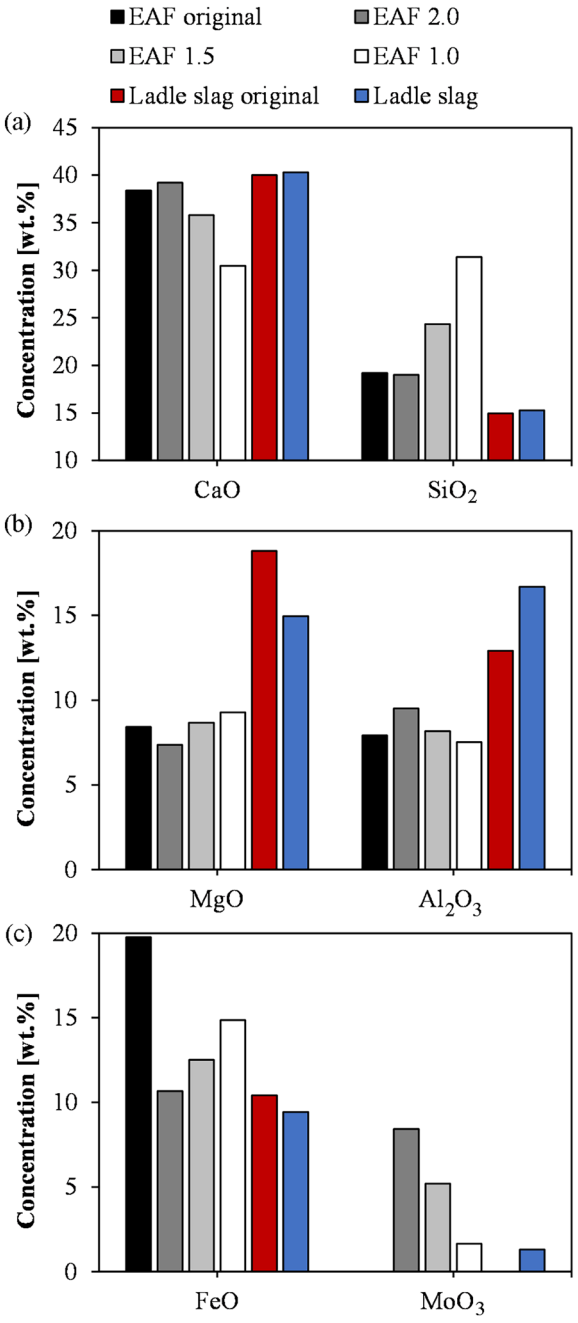

Fig. 3 Analyzed concentration of **a** CaO, SiO_2, **b** MgO, Al_2O_3, **c** FeO, and MoO_3 in each slag determined by XRF. The legend applies to all three figures

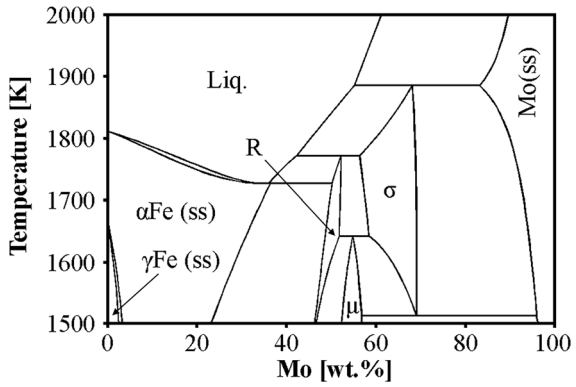

Fig. 4 Fe-Mo binary phase diagram. Calculated using the phase diagram module of FactSage 8.2 with the FSstel database [29]

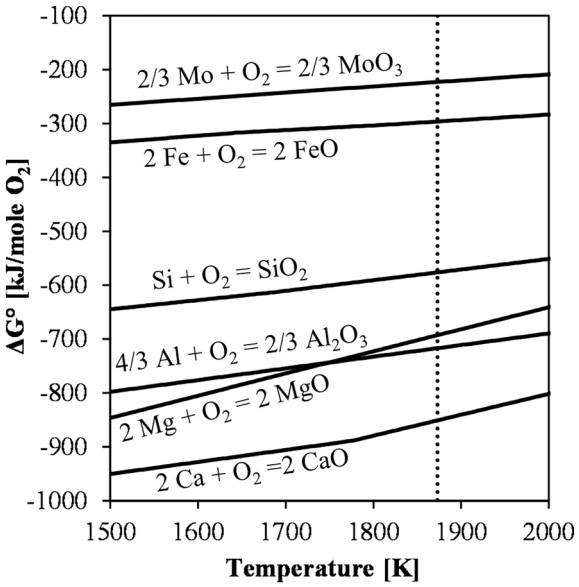

Fig. 5 Oxygen potential diagram where the dashed line represents the experimental temperature during remelting. Calculated using FactSage 8.2 and the FactPS database [29]

and MoO_3. Thus, the presence of ferric iron might induce oxidation of the crucible. However, the molten slag phase is a concentrated solution phase, i.e., not pure substances as shown in the oxygen potential diagram. Figure 3c unambiguously shows that the phase equilibria allow for the reduction of the ferrous iron in the slag by the molybdenum crucible at the present conditions. Consequently, the oxidation state of iron in the slag was more likely buffered between metallic and ferrous iron rather than ferrous and ferric iron.

By adding silica in increasing amounts, the concentrations of CaO and Al_2O_3 were consistently diluted, Fig. 3. In contrast, the MgO content seemingly increased, which, naturally, should be disregarded as an actual phenomenon. The silica modification generated slags with B2 basicities of 1.47 and 0.97, which satisfies the desired outcome. The interaction with the molybdenum was observed for both modified slags, although in decreasing extents with decreasing basicities. Adding silica lowers the overall concentration—and possibly activity—of MeO-type network breakers, which can be assumed to lower the driving force of Eq. 1 in the right direction.

The remelted ladle slag was analyzed for similar CaO and SiO_2 concentrations, Fig. 3. However, both the MgO and Al_2O_3 contents were somewhat different, which, again, should not be seen as an actual phenomenon of remelting and granulating from molybdenum crucibles. The FeO content of the ladle slag was lower than that of the original EAF slag, which might contribute to the lesser extent of interaction with the crucible even though the basicity of the slag was high.

A common approach to minimize slag-crucible interactions in pyrometallurgical experiments is to use a ceramic system and saturate the slag with the component representing the crucible. This approach is suitable for studying steelmaking slags already saturated in magnesia for minimizing refractory wear, as demonstrated by, e.g., Lee and Fruehan [30]. Employing magnesia crucibles in the present study would allow for less significant interactions at higher basicities. However, the granulation aspect would prove challenging as the crucibles were handled manually. Nonetheless, the compositions achieved after water granulation using molybdenum crucibles were considered satisfactory to address the aim of the present study.

Phase Distributions

The phase distribution generated by solidification under the assumption of infinitely fast solute redistribution in the liquid phase and no diffusion in the solid state was calculated using a Scheil-Gulliver-type thermodynamic calculation. The results in Fig. 6 show that modification of the EAF slag lowers the liquidus temperature and changes the primary crystallization field from the MeO-type solid solution to spinel. Furthermore, from a thermodynamic standpoint, the non-modified EAF slag has MeO (ss) present at the remelting temperature of 1873 K, which is consistent with the industrial operation aiming at minimizing refractory wear. The same can be stated for the ladle slag, although this slag has an even higher portion of solid MeO (ss) at the experimental temperature.

The diffractograms of the milled water-granulated slags with 10 wt% corundum as an internal standard are presented in Fig. 7. Compared to the thermodynamic calculations presented in Fig. 6, the overall results are consistent between thermodynamics and experiments. More specifically, MeO (ss), represented by magnesiowüstite, is the first phase to crystallize, and dicalcium silicate co-precipitates upon further cooling. However, there is a discrepancy between the calculations and observations for EAF 1.0 as spinel is the primary phase to crystallize from a thermodynamic standpoint.

In terms of the phase distribution, the Rietveld refinement indicated that EAF 2.0 contained 7, 17, and 76 wt% MeO (ss), α′-dicalcium silicate, and amorphous material,

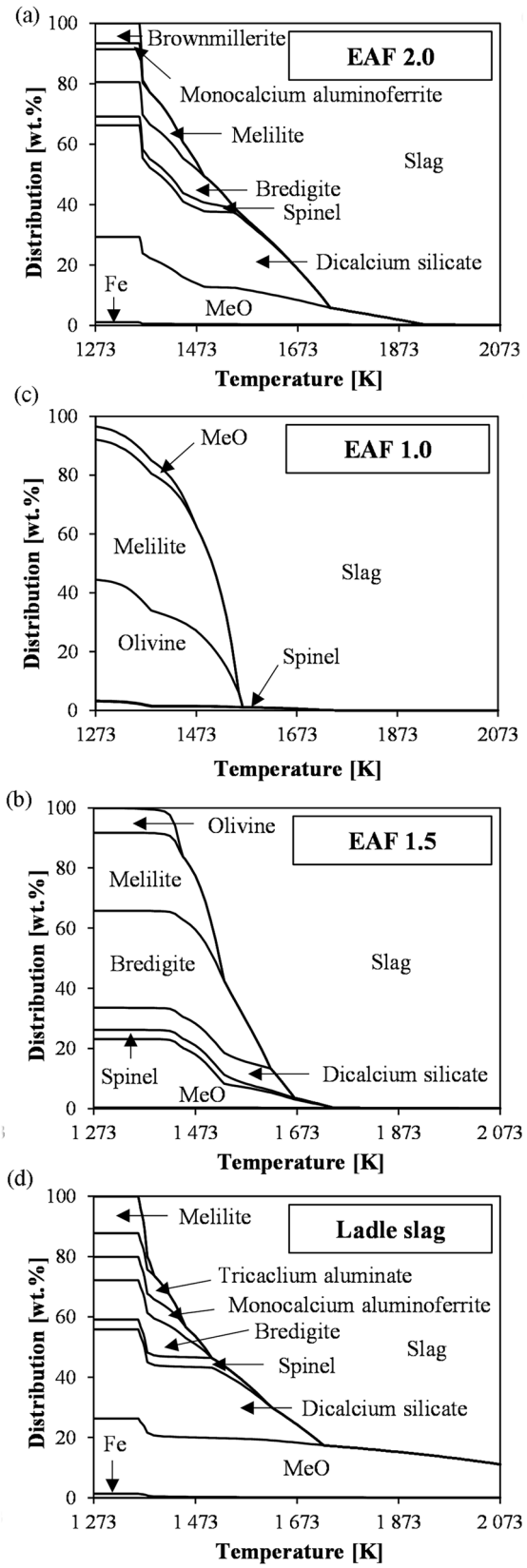

Fig. 6 Results from Scheil-Gulliver cooling calculations for **a** EAF 2.0, **b** EAF 1.5, and **c** EAF 1.0. Calculated using the Equilib module of FactSage 8.2 using the databases FactPS and FToxid [29]

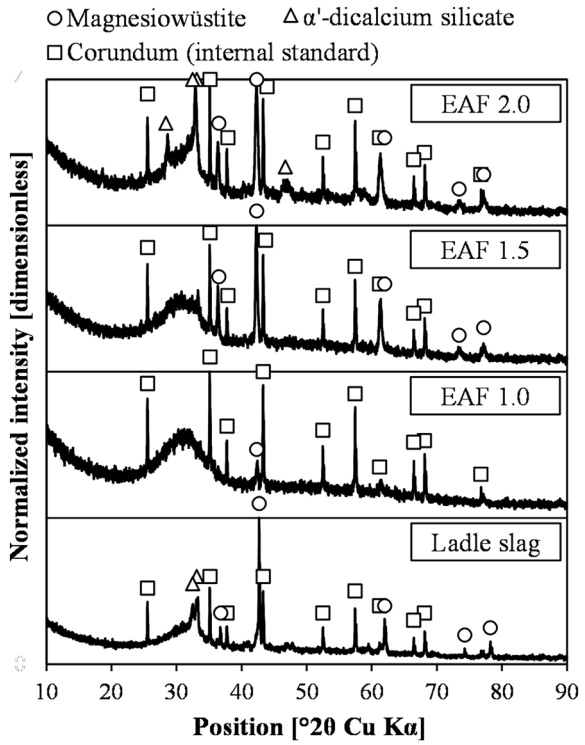

Fig. 7 Diffractograms of the water granulated samples with 10 wt% corundum as internal standard

respectively. Furthermore, the ladle slag was comprised of 14, 17, and 69% MeO (ss), α′-dicalcium silicate, and amorphous material, respectively. Thus, the distribution between the crystalline phases, i.e., the ratio between MeO (ss) and dicalcium silicate, is consistent with the continuous cooling calculations presented in Fig. 6. In line with Deng et al. [31], increased polymerization of slags demotes ion migration and increases the energy barrier for crystallization, which is apparent for the lower basicity slags EAF 1.5 and EAF 1.0. The amorphous contents of these slags were estimated to be 93 and 96 wt% for EAF 1.5 and EAF 1.0, respectively; the remaining percentages were constituted by MeO (ss). In addition to the structural aspect, the temperature window constituted by the difference in the liquidus and experimental temperature is correlated to the estimated amorphous contents of the slags.

The SEM–EDS analyses were used to estimate the chemical composition of the amorphous phase and verify the observations from the XRD. The latter was achieved qualitatively by the microstructure and EDS analyses. Figure 8 illustrates the micrographs of the water-granulated EAF slags and ladle slag. The global microstructure of the granules of each EAF slag was similar to that of EAF 2.0, which is depicted in Fig. 8a; the low magnification micrographs of the remaining EAF slags were thus omitted to avoid repetition. The ladle slag differed from the EAF slag by its presence of the MeO (ss) phase that, judging from the microstructure, was present already prior to the granulation, see entrained darker phase in Fig. 8b. Apart from the MeO (ss) in the ladle slag, no crystalline microstructure was observed at lower magnifications, i.e., the EAF slags and ladle slag appeared amorphous.

The microstructures at higher magnification of larger granules with severe crystallization are included in Fig. 8c–f. Combining the XRD data with the SEM–EDS analyses, a portion of the granules of the EAF slags can be stated to consist of a glassy matrix with microcrystalline phases. Thus, the rapid quenching did not allow significant growth of the crystals.

Areas of the amorphous phase, i.e., areas free from crystalline phases at the polished surface, were analyzed by EDS to estimate the composition of the glassy portion of the four samples. Table 3 presents the average concentration recalculated to oxides based on 20 EDS spectrums for each sample. Compared to Fig. 3, the overall compositions are consistently represented, and the silica modification generated logical trends for the dilution of other components. Furthermore, the lower MgO contents of the amorphous phase of EAF 2.0, EAF 1.5, and ladle slag correspond to the MeO (ss) crystallization.

Regarding the crystalline phases, the MeO (ss) of the ladle slag was estimated to represent $(Mg_{0.9}, Fe_{0.1})O$. On the other hand, the EAF slags' microcrystalline phases were too small to maintain the electron beam's interaction volume within a single phase. Therefore, the EDS analyses of these phases were used in combination with the underlying glass composition to estimate what elements could be attributed to the crystallized material. The analyzed crystals in EAF 2.0 and EAF 1.5 were attributed to MeO (ss) as the EDS spectrums were enriched in MgO and FeO as compared to the amorphous phase. The lighter phases of Fig. 8e were rich in chromium, which suggests a spinel phase. These observations are consistent with the thermodynamic calculations presented in Fig. 6. However, no distinction of the dicalcium silicate phase could be determined based on the EDS, possibly due to the similarity in calcium to silicon ratio in the amorphous phase. In addition, MeO (ss) was not found in EAF 1.0, which is consistent with the thermodynamic calculations but deviates from the XRD. Possibly, the qualitative nature of the SEM–EDS failed to include MeO (ss), while the detection limit of the XRD was below the concentration of the spinel.

Based on the chemical composition of the slags, the degree of polymerization was estimated by calculating the quotient of non-bridging oxygen to tetragonally coordinated oxygen (NBO/T) according to [32]. These calculations were performed for the original EAF slag, the theoretical compositions of the modified EAF slags, the original ladle slag, and the amorphous phases determined by the EDS analyses.

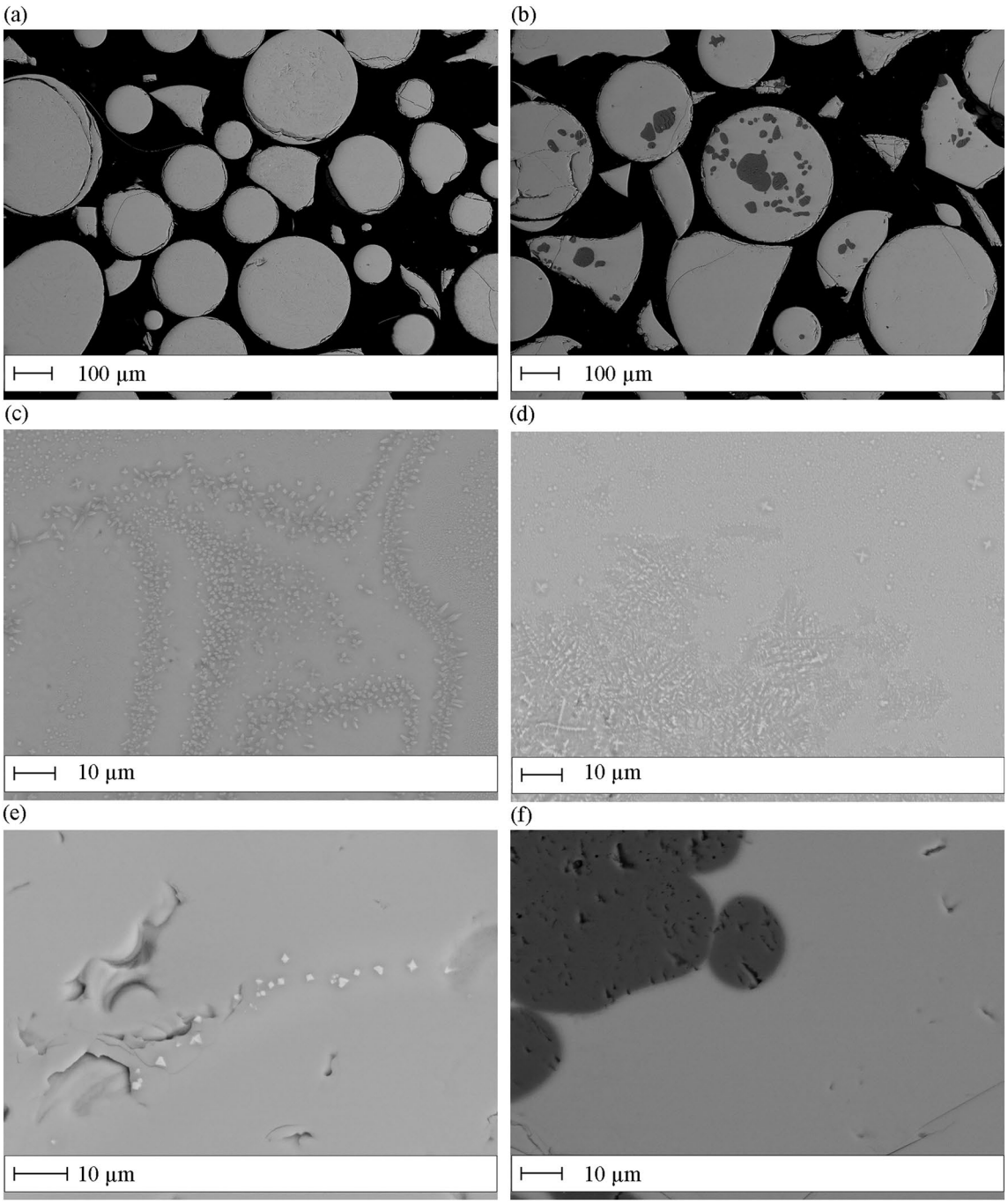

Fig. 8 Angle selective backscattered images representing **a** EAF 2.0, **b** ladle slag, **c** EAF 2.0, **d** EAF 1.5, **e** EAF 1.0, and **f** ladle slag

Table 3 Average glass composition [wt%] of 20 EDS analyses per sample presented in wt%. P_2O_5 was excluded from the table

Sample	CaO	SiO_2	MgO	Al_2O_3	FeO	MnO	TiO_2	Cr_2O_3	MoO_3
EAF 2.0	41.7	18.4	5.0	8.6	11.4	3.9	1.3	0.6	9.1
EAF 1.5	36.9	22.9	7.4	7.5	13.4	3.8	1.1	0.7	5.9
EAF 1.0	31.5	30.2	8.0	6.5	16.4	3.4	1.0	0.8	2.0
Ladle slag	47.4	15.3	6.9	15.6	10.4	1.2	0.7	0.3	2.3

The results show that despite the crystallization of network-breaking oxides, the higher basicity samples still have more depolymerized amorphous phases, see Table 4, which is positive for reactivity in SCM applications [4, 11].

Based on the characterization of the slags, implications related to employing future steelmaking slags as SCMs can be highlighted. Although the granulation of the non-modified EAF slag generated significantly higher glass contents than previously achieved [33], the crystallization of phases highlights that granulating such a depolymerized slag to a glassy material is not straightforward. Mind that the present granulation setup has been shown to achieve the same amorphous content as an industrial setup for iron silicate slags [34]. Naturally, the implications are partly positive if phases with hydraulic properties crystallize. However, when MgO dominant MeO (ss) forms, the SCM will be less attractive, especially if the hydration of the MgO is delayed in relation to the setting of the concrete. The hydration to $Mg(OH)_2$ is associated with an expansion of the solid volume, which damages the concrete if the stress generated by the expansion exceeds the tensile strength of the concrete [35]. The effect might be mitigated by fine milling [35] or if the MeO (ss) is stabilized by higher FeO contents in the solid solution [36].

Performance as Supplementary Cementitious Material

The iterative milling of the granulated samples generated specific surface areas close to 1.2 m^2/g as presented in Table 5. The similar areas propose that differences in reactivities should be attributed to characteristics other than granulometric properties. However, for the comparison with the two commercial GGBS samples, attention should be paid to the differences in specific surface areas. In addition, the inert material quartz had the lowest specific surface area.

In the isothermal calorimetry-based testing, the temperatures of the samples were allowed to stabilize for 45 min before considering the signals to be correct. Clearly, the peaks of the heat flow for EAF 2.0 and the ladle slag were reached within these first 45 min as the derivates of the curves are negative from $t = 0$ h, see Fig. 9. Nonetheless, even though the maximum was missed, the absolute values of the heat flow were highest for these two samples in the tested series. Based on the XRD, these two samples contained α′-dicalcium silicate, which is a high-temperature orthorhombic polymorph of dicalcium silicate, or Belite, an important clinker phase in Portland cement [37]. Therefore, the results suggest that the presence of this hydraulic phase contributed to the high heat flows.

For the two samples with amorphous contents in a similar range and without α′-dicalcium silicate, viz. EAF 1.5 and EAF 1.0, the lower degree of polymerization calculated for EAF 1.5 indicate a higher reactivity during the first 24 h, compare Table 4 and Fig. 9. This is consistent with reported literature on other systems showing increasing reactivities for more depolymerized glass [4, 11].

The juxtaposition of the GGBS, EAF, and ladle slags suggests that the GGBS have a different reaction behavior. The GGBS samples have two peaks in the recorded heat flow, which could constitute the phase assemblage of calcium silicate hydrate and calcium aluminum silicate hydrate gels, as

Table 4 NBO/T calculated for the whole slag (whole) and the analyzed amorphous phase (glass)

Sample	NBO/T (whole)	NBO/T (glass)
EAF 2.0	4.71	4.04
EAF 1.5	3.86	3.70
EAF 1.0	2.84	3.02
Ladle slag	4.79	3.61

Table 5 BET specific surface area of the milled samples

Sample	BET [m^2/g]
EAF 2.0	1.19
EAF 1.5	1.20
EAF 1.0	1.21
Ladle slag	1.20
GGBS1	1.44
GGBS2	1.63
Quartz	0.45

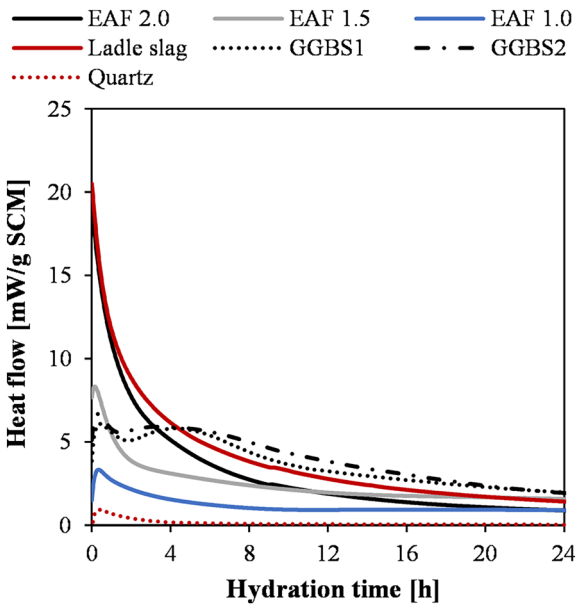

Fig. 9 Heat flow during the first 24 h of the isothermal calorimeter experiment

well as the formation of alumina ferric oxide tri-substituted and mono-substituted [27, 28]. In tricalcium silicate systems, the influence of alumina was shown by Zhang et al. [38] to depend on the availability of SO_4^{2-} and Al^{3+} in solution. This was translated to, i.a., the concentration of alumina in the sample [38]. In the present study, the GGBS samples had higher alumina contents as compared to the EAF slags, which might constitute the difference. Furthermore, for the ladle slag, the effect of alumina might be invisible based on the heat flow due to the heat generated from the hydration of the α′-dicalcium silicate phase.

The cumulative heat over 7 days is presented in Fig. 10, and the results show that the materials are most reactive in the following order GGBS1, ladle slag, GGBS2, EAF 1.5, EAF 2.0, EAF 1.0, and quartz. A noteworthy observation is the slopes of EAF 1.5 and EAF 1.0 towards the final part of the experiment. These slopes indicate that EAF 1.5 and EAF 1.0 are continuously contributing to a higher heat flow as compared to the other samples. Consequently, these compositions might perform better in a longer time frame.

The cumulative heat of EAF 2.0 and ladle slag presented in Fig. 10 reflect the phase distribution and composition of the glass phases. Both samples show a high initial heat flow from the α′-dicalcium silicate. Subsequently, the ladle slag progresses to a higher cumulative heat due to its higher alumina content, despite having a more polymerized glass phase. Compared to EAF 1.5 and EAF 1.0, the initially lower progressions of the cumulative heat stem from the absence of α′-dicalcium silicate. However, the high amorphous content of EAF 1.5 allowed this slag to surpass the cumulative heat of EAF 2.0. In contrast, EAF 1.0 did not have a higher reactivity than EAF 2.0 within 7 days despite its higher amorphous content. This discrepancy can be attributed to the difference in degree of polymerization, Table 4.

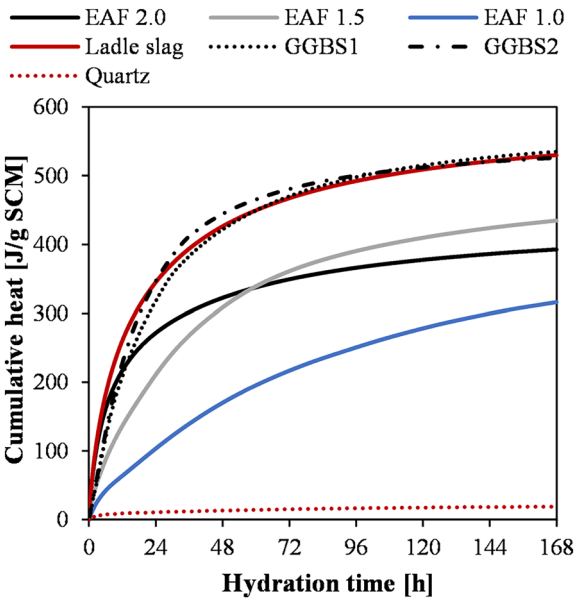

Fig. 10 Cumulative heat recorded in the isothermal calorimeter experiment

Figure 10 shows that the reactivity of the inert reference, i.e., quartz, is distinguished from all other samples; therefore, this measurement will not be addressed further. GGBS was included as a reference material representing a recognized SCM from the iron and steelmaking industry. Ideally, an established SCM with lower reactivity than GGBS should have been included in the study to offer a basis for comparing the lower spectrum of reactivity. However, since the R^3 test has been shown to have high repeatability between laboratories [6], previously published values for fly ash were included as a comparison. Siliceous fly ashes from coal combustion have been shown to have reactivities within the range of 163 and 214 J/g SCM [6], which is less than EAF 1.0. Therefore, all four slag samples in the present study are of interest for the SCM application from a reactivity standpoint.

In terms of the comparison to GGBS, Table 6 includes reactivity values after 7 days of hydration normalized per mass and specific surface area. Considering the latter value, i.e., normalized per surface area, both EAF 2.0 and EAF 1.5 are indicated to have the potential to generate similar reactivities as GGBS if milled further. EAF 2.0 was partially benefited by its hydraulic crystalline phase, while EAF 1.5 has a lower degree of polymerization than the GGBS samples; compare NBO/T of 3.86 for EAF 1.5 to 2.13 and 1.77 for GGBS1 and GGBS2, respectively.

The sample of the present study with the most similar composition to the GGBS samples is EAF 1.0, see Fig. 11. Compared to GGBS2, the B2 basicity is similar, while the main difference is the FeO content followed by the concentration in alumina. The role of FeO in SCMs is not fully understood [23, 28]. However, although alumina is associated with higher reactivity, the comparison of EAF 1.0 and GGBS2, see Table 6, indicates that FeO is detrimental to the reactivity. The pH value in cement pore solution conditions has been reported to span 12.4 to 13.5 [39]. Therefore, considering that iron is not keen on dissolving at these basic pH levels, Fig. 12, it is likely that FeO contents in the

Table 6 Cumulative heat after 7 days of hydration

Sample	$Heat_{7D}$ [J/g]	$Heat_{7D}$ [J/m^2]
EAF 2.0	393	331
EAF 1.5	435	362
EAF 1.0	316	262
Ladle slag	530	443
GGBS1	535	372
GGBS2	526	323

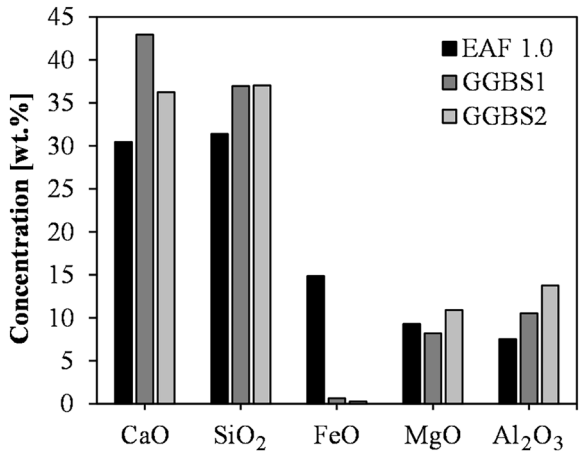

Fig. 11 Comparison of chemical compositions of EAF 1.0, GGBS1, and GGBS2

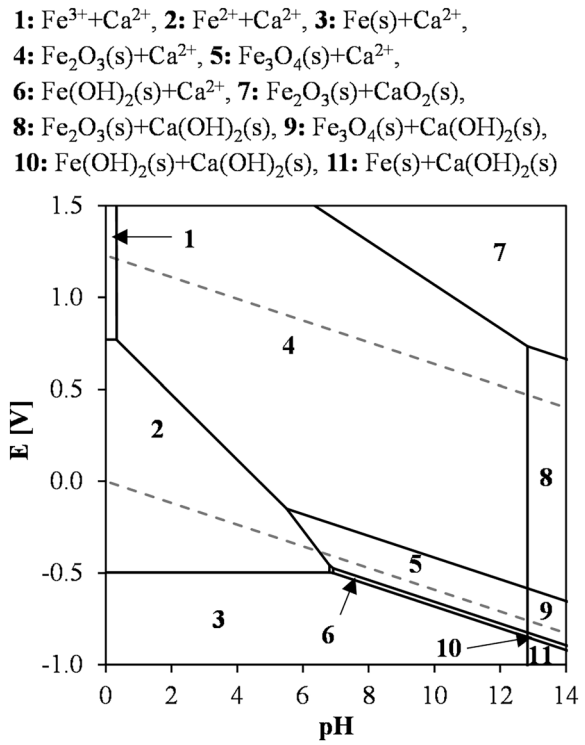

Fig. 12 EpH diagram of the Fe–Ca–O–H system at 298.15 K and 0.001 molality for the solutes, calculated using the EpH module of FactSage 8.2. The dashed lines represent the water stability area

slag are hampering the dissolution rate of the material. This observation necessitates future studies for verification and identification of mechanisms.

The observations related to FeO and the crystallization experienced by the non-modified EAF slag imply that utilizing EAF slags as highly reactive SCMs will be preceded by choices in modification related to silica content and reduction of FeO. If the industrial water granulation fails to generate an amorphous slag free from crystallization of MeO (ss) rich in MgO, silica modification can be performed to move away from the primary crystallization field of MeO (ss), as shown in Fig. 6a–c. The reduction of FeO to avoid potential hampering of reactivity for GGBS-type compositions rich in FeO can be employed after modifications in silica. For the industrial aspect, energy balances and choice of refractory have to be considered for such operations. In addition, since FeO is a fluxing component at high basicities, the order of the modifications has to be considered.

Conclusions

The present study addressed the valorization of EAF slag as a supplementary cementitious material in the context of ore-based EAF operation using HBI. Based on the experimental work, the following was concluded:

- Water-granulated EAF slag with a basicity of 2.0 was found to have 76 wt% amorphous content in addition to crystalline α′-dicalcium silicate and MeO (ss), which resulted in a reactive SCM, indicating the possibility of reaching similar performance as GGBS due to a depolymerized amorphous phase and hydraulic crystalline phase.
- Water-granulated silica-modified EAF slag with a basicity of 1.5 was found to have an amorphous content of 93 wt% and crystalline MeO (ss), which resulted in a high-performing SCM, indicating the possibility of reaching similar reactivities as GGBS due to the depolymerized amorphous phase.
- Water-granulated silica-modified EAF slag with a basicity of 1.0 was found to have an amorphous content of 96 wt% and crystalline MeO (ss), but the resulting reactivity was not indicated to be able to reach GGBS although having a similar composition, which was indicated to be related to the FeO content in the glass phase of the EAF slag.

Therefore, the valorization of EAF slags in general, and future EAF slags from hydrogen-based ironmaking in particular, as high-performing SCMs will partly be a challenge in balancing the detrimental crystallization of MeO-type solid solution rich in magnesia and addressing the iron oxide content in the amorphous phase.

Acknowledgements The assistance of Britt-Louise Holmqvist is greatly acknowledged.

Funding Open access funding provided by Lulea University of Technology. This study was financed by Resource via Vinnova and the

Swedish Energy Agency and the work was conducted within the Center of Advanced Mining and Metallurgy (CAMM) at Luleå University of Technology.

Declarations

Conflict of interest The authors declare that they have no conflict of interest.

References

1. Pei M, Petäjäniemi M, Regnell A, Wijk O (2020) Toward a fossil free future with HYBRIT: development of Iron and steelmaking technology in Sweden and Finland. Metals 10:972. https://doi.org/10.3390/met10070972
2. EUROSLAG (2018) Statistics 2018. https://www.euroslag.com/research-library-downloads/downloads/ Accessed 6 Oct 2023
3. Strandkvist I, Pålsson K, Andersson A, Olofsson J, Lennartsson A, Samuelsson C, Engström E (2020) Minimizing chromium leaching from low-alloy electric arc furnace (EAF) slag by adjusting the basicity and cooling rate to control brownmillerite formation. Appl Sci 10:35. https://doi.org/10.3390/app10010035
4. Skibsted J, Snellings R (2019) Reactivity of supplementary cementitious materials (SCMs) in cement blends. Cem Concr Res 124:105799. https://doi.org/10.1016/j.cemconres.2019.105799
5. Lothenbach B, Scrivener K, Hooton RD (2011) Supplementary cementitious materials. Cem Concr Res 41:1244–1256. https://doi.org/10.1016/j.cemconres.2010.12.001
6. Li X, Snellings R, Antoni M, Alderete NM, Ben Haha M, Bishnoi S, Cizer Ö, Cyr M, De Weerdt K, Dhandapani Y, Duchesne J, Haufe J, Hooton D, Juenger M, Kamali-Bernard S, Kramar S, Marroccoli M, Joseph AM, Parashar A, Patapy C, Provis JL, Sabio S, Santhanam M, Steger L, Sui T, Telesca A, Vollpracht A, Vargas F, Walkley B, Winnefeld F, Ye G, Zajac M, Zhang S, Scrivener KL (2018) Reactivity tests for supplementary cementitious materials: RILEM TC 267-TRM phase 1. Mater Struct 51:151. https://doi.org/10.1617/s11527-018-1269-x
7. Kucharczyk S, Sitarz M, Zajac M, Deja J (2018) The effect of CaO/SiO_2 molar ratio of $CaO–Al_2O_3–SiO_2$ glasses on their structure and reactivity in alkali activated system. Spectrochim Acta A Mol Biomol Spectrosc 194:163–171. https://doi.org/10.1016/j.saa.2018.01.018
8. Glosser D, Suraneni P, Burkan Isgor O, Jason Weiss W (2021) Using glass content to determine the reactivity of fly ash for thermodynamic calculations. Cem Concr Compos 115:103849. https://doi.org/10.1016/j.cemconcomp.2020.103849
9. Snellings R (2013) Solution-controlled dissolution of supplementary cementitious material glasses at pH 13: the effect of solution composition on glass dissolution rates. J Am Ceram Soc 96:2467–2475. https://doi.org/10.1111/jace.12480
10. Ramanathan S, Perumal P, Illikainen M, Suraneni P (2021) Mechanically activated mine tailings for use as supplementary cementitious materials. RILEM Tech Lett 6:61–69. https://doi.org/10.21809/rilemtechlett.2021.143
11. Schöler A, Winnefeld F, Ben Haha M, Lothenbach B (2017) The effect of glass composition on the reactivity of synthetic glasses. J Am Ceram Soc 100:2553–2567. https://doi.org/10.1111/jace.14759
12. Ramanathan S, Tuen M, Suraneni P (2022) Influence of supplementary cementitious material and filler fineness on their reactivity in model systems and cementitious pastes. Mater Struct 55:136. https://doi.org/10.1617/s11527-022-01980-2
13. Rojas MF, Sánchez de Rojas MI (2004) Chemical assessment of the electric arc furnace slag as construction material: expansive compounds. Cem Concr Res 34:1881–1888. https://doi.org/10.1016/j.cemconres.2004.01.029
14. Hekal EE, Abo-El-Enein SA, El-Korashy SA, Megahed GM, El-Sayed TM (2013) Hydration characteristics of Portland cement–electric arc furnace slag blends. HBRC J 9:118–124. https://doi.org/10.1016/j.hbrcj.2013.05.006
15. Muhmood L, Vitta S, Venkateswaran D (2009) Cementitious and pozzolanic behavior of electric arc furnace steel slags. Cem Concr Res 39:102–109. https://doi.org/10.1016/j.cemconres.2008.11.002
16. Alsheltat MF, Elfigih MA (2023) Effects of electric arc furnace slag powder and fly ash within ternary waste blend on performance of concrete. Open Ceram 14:1–9. https://doi.org/10.1016/j.oceram.2023.100359
17. Lee JY, Choi JS, Yuan TF, Yoon YS, Mitchell D (2019) Comparing properties of concrete containing electric arc furnace slag and granulated blast furnace slag. Maters 12:1371. https://doi.org/10.3390/ma12091371
18. Amin MS, El-Gamal SMA, Abo-El-Enein SA, El-Hosiny FI, Ramadan M (2015) Physico-chemical characteristics of blended cement pastes containing electric arc furnace slag with and without silica fume. HBRC J 11:321–327. https://doi.org/10.1016/j.hbrcj.2014.07.002
19. Roslan NH, Ismail M, Abdul-Majid Z, Ghoreishiamiri S, Muhammad B (2016) Performance of steel slag and steel sludge in concrete. Constr Build Mater 104:16–24. https://doi.org/10.1016/j.conbuildmat.2015.12.008
20. Kim HS, Kim KS, Jung SS, Hwang JI, Choi JS (2015) Valorization of electric arc furnace primary steelmaking slags for cement applications. Waste Manag 41:85–93. https://doi.org/10.1016/j.wasman.2015.03.019
21. Bullerjahn F, Bolte G (2022) Composition of the reactivity of engineered slags from bauxite residue and steel slag smelting and use as SCM for Portland cement. Constr Build Mater 321:1–15. https://doi.org/10.1016/j.conbuildmat.2022.126331
22. Mostaghel S (2012) Influence of alumina on the zinc slag fuming processes: an experimental study on physical properties and leaching behaviour of the generated fayalite-type slag. Doctoral thesis, Luleå University of Technology, pp 20
23. Astoveza J, Trauchessec R, Migot-Choux S, Soth R, Pontikes Y (2022) Iron-rich slag addition in ternary binders of Portland cement, aluminate cement and calcium sulfate. Cem Concr Res 153:106689. https://doi.org/10.1016/j.cemconres.2021.106689
24. Moon GD, Oh S, Choi YC (2016) Effects of the physicochemical properties of fly ash on the compressive strength of high-volume fly ash mortar. Constr Build Mater 124:1072–1080. https://doi.org/10.1016/j.conbuildmat.2016.08.148
25. Snellings R, Scrivener KL (2016) Rapid screening tests for supplementary cementitious materials: past and future. Mater Struct 49:3265–3279. https://doi.org/10.1617/s11527-015-0718-z
26. Avet F, Snellings R, Diaz AA, Ben Haha M, Scrivener K (2016) Development of a new rapid, relevant and reliable (R^3) test

method to evaluate the pozzolanic reactivity of calcined kaolinitic clays. Cem Concr Res 85:1–11. https://doi.org/10.1016/j.cemconres.2016.02.015
27. Sivakumar PP, Matthys S, De Belie N, Gruyaert E (2021) Reactivity assessment of modified Ferro silicate slag by R^3 method. Appl Sci 11:336. https://doi.org/10.3390/app11010366
28. Hallet V, De Belie N, Pontikes Y (2020) The impact of slag fineness on the reactivity of blended cements with high-volume non-ferrous metallurgy slag. Constr Build Mater 257:119400. https://doi.org/10.1016/j.conbuildmat.2020.119400
29. Bale CW, Bélisle E, Chartrand P, Decterov SA, Eriksson G, Gheribi AE, Hack K, Jung IH, Kang YB, Melançon J, Pelton AD, Petersen S, Robelin C, Sangster J, Spencer P, Van Ende MA (2016) Reprint of: FactSage thermochemical software and databases, 2010–2016. Calphad 55:1–19. https://doi.org/10.1016/j.calphad.2016.07.004
30. Lee CM, Fruehan RJ (2005) Phosphorus equilibrium between hot metal and slag. Ironmak Steelmak 32:503–508. https://doi.org/10.1179/174328105X48142
31. Deng L, Yao B, Lu W, Zhang M, Li H, Chen H, Zhao M, Du Y, Zhang M, Ma Y, Wang W (2022) Effect of SiO_2/Al_2O_3 ratio on the crystallization and heavy metal immobilization of glass ceramics derived from stainless steel slag. J Non Cryst Solids 593:121770. https://doi.org/10.1016/j.jnoncrysol.2022.121770
32. Mills KC (1995) Structure of liquid slags. In: Springorum D (ed) Slag atlas, 2nd edn. Verlag Stahleisen GmbH, Düsseldorf, pp 1–8
33. Tossavainen M, Engstrom F, Yang Q, Menad N, Lidstrom Larsson M, Bjorkman B (2007) Characteristics of steel slag under different cooling conditions. Waste Manag 27:1335–1344. https://doi.org/10.1016/j.wasman.2006.08.002
34. Andersson A, Brander L, Lennartsson A, Roos Å, Engström F (2023) A method for synthesizing iron silicate slags to evaluate their performance as supplementary cementitious materials. Appl Sci 13:8357. https://doi.org/10.3390/app13148357
35. Song Q, Su J, Nie J, Li H, Hu Y, Chen Y, Li R, Deng Y (2021) The occurrence of MgO and its influence on properties of clinker and cement: a review. Constr Build Mater 293:123494. https://doi.org/10.1016/j.conbuildmat.2021.123494
36. Strandkvist I, Sandström Å, Engström F (2017) Effect of FeO/MgO ratio on dissolution and leaching of magnesiowüstite. Steel Res Int 88:1600322. https://doi.org/10.1002/srin.201600322
37. Ludwig HM, Zhang W (2015) Research review of cement clinker chemistry. Cem Concr Res 78:24–37. https://doi.org/10.1016/j.cemconres.2015.05.018
38. Zhang Y, Wan Z, de Lima Junior LM, Çopuroğlu O (2022) Early age hydration of model slag cement: interaction among C_3S, gypsum and slag with different Al_2O_3 contents. Cem Concr Res 161:106954. https://doi.org/10.1016/j.cemconres.2022.106954
39. Andersson K, Allard B, Bengtsson M, Magnusson B (1989) Chemical composition of cement pore solutions. Cement Concr Res 19:327–332. https://doi.org/10.1016/0008-8846(89)90022-7